

## PART A: EXPERIMENTAL INVESTIGATION OF UNSTEADY SUPERCAVITATING FLOWS\*

A. RABIEE<sup>1, \*\*</sup>, M. M. ALISHAHI<sup>2</sup>, H. EMDAD<sup>3</sup> AND B. SARANJAM<sup>4</sup>

<sup>1,2,3</sup> Department of Mechanical Engineering, Shiraz University, Shiraz, I. R. of Iran  
Email: rabiee@shirazu.ac.ir

<sup>4</sup> Malek-Ashtar University of Technology, Shiraz, I. R. of Iran

**Abstract**– The present experimental study is the first part of an investigation of unsteady cavitating flows. In the second part, the proper numerical modeling of such flow fields is introduced in order to remove the deficiencies of customary computational models. This study focuses on supercavitation initiation and its transitional process to partial cavitation and, finally, noncavitating flow as the body bears acceleration from rest and deceleration in a water test tank. Using a high speed camera, cavitation bubble status and motion characteristics of the body displacement after being launched in the prepared test tank are recorded and extracted. After processing the recorded images, body motion parameters including, speed, acceleration and consequently the total drag force in addition to cavitation bubble length and diameter were derived. Due to the high acceleration imposed on the body (7000g), during the short interval of launching time, the model design is a complex process compromising low weight and high strength. Some aspects of the test set up and model modification, as well as the proper data processing are explained in this paper.

From the experiments, it is observed that in the accelerating phase, as the velocity increases it is equivalent to lowering the cavitation number, the length of cavitation bubble is also increased, which is consistent with the expectations. However, in the decelerating phase this trend is reversed, which is totally unexpected. Finally, the experimental results are compared with the results of steady state flow field solutions and the difference between the two sets of results is huge. This deficiency is related to the dynamics of unsteady cavitating flow that is discussed in the second part of this paper.

**Keywords**– Cavitation, experiment, unsteady

### 1. INTRODUCTION

In liquid flows, cavitation generally happens if the pressure in certain locations drops below the vapor pressure and consequently the negative pressures are relieved by the formation of gas-filled or gas- and vapor-filled cavities [1]. Cavitation can be seen in a wide variety of propulsion and power systems like pumps, injectors, nozzles, marine propellers, hydrofoils and underwater bodies [2]. Apart from the damage associated with cavitation such as vibrations, noise, performance alterations, erosion and structural damages, there are applications in which one can see the beneficial effects of cavitation. High-speed hydrofoil boats, supercavitating propellers and supercavitating vehicles are some examples. By generating supercavitation around hydrodynamic vehicles, skin-friction drag can be decreased substantially. To achieve these goals, accurate and detailed information of the flow field is required [3, 4].

Besides the numerical methods, various experimental techniques have been developed to study the flow structure and modeling issues to modify numerical cavitation models [5, 6].

From the early works on cavitation, Rouse and McNown [6] can be mentioned. Although they did not report about the time dependency of their work, their experimental results have been mostly used by

---

\*Received by the editors February 4, 2010; Accepted August 18, 2010.

\*\*Corresponding author

others. Considered geometries included a cylindrical after-body with a hemispherical nose. They reported pressure distributions on such bodies at different Reynolds and cavitation numbers.

Arakeri and Acosta [7] studied the cavitation inception and development on two axisymmetric bodies using the Schlieren flow visualization method. Cavitation inception was found to occur in the laminar boundary layer separation region. Actually, there is a close connection between the point of laminar separation and cavity detachment. Arakeri [8] also explained the role of viscosity during smooth cavity separation and showed that the distance between these two points is strongly dependent on the Reynolds number.

Franc and Michel [9] investigated this issue further by studying the cavitating flow over circular, elliptic cylinders and NACA foils. The visualization of the boundary layer with dye injection showed that there is a strong interaction between the attached cavitation and the boundary layer.

Kawanami et al. [10] conducted a series of experiments to control the cloud cavitation as one of the unsteady and unstable regimes. It was demonstrated that re-entrant jet downstream of the cavity is the basic mechanism that triggers the shedding of the cloud cavitation. They reported that this process can be controlled by adding a small obstacle to block the re-entrant jet. Cavitation noise and drag can be decreased effectively by this modification on the hydrofoil surface.

At a sufficiently low cavitation number, supercavitation occurs when the size of the cavity covers the entire underwater object. Compared with the other types of cavitation, in this regime, there is often a distinct interface between the main flow and the cavitating region. In recent years, supercavitation research has attracted growing interest due to its potential for vehicle maneuvering and drag reduction, [11, 12]. In this way, Li et. al. [13] used high speed video camera with PIV measurements for resolving flow field such as velocity and vorticity distributions about the hydrofoil, particularly in supercavitation regime.

High speed images of supercavitating underwater projectiles traveling up to and exceeding the speed of sound in water were conducted by Hrubec [14] in short-range vehicles. Projectiles were launched at high speed in an instrumented underwater test range providing critical data to support basic research in supercavitating bodies. These images revealed information on projectile flight behavior, stability, cavity shape, diameter and length of cavitation region, and in-barrel launch characteristics.

Schaffar et al [15] presented some experimental results on supercavitating projectiles. These experiments were carried out within the framework of a feasibility program to find out the problems of high speed projectiles. They tested different shapes of cavitator for several angles of attack and determined that for small angles, up to  $5^\circ$ , the trajectory of the body can be corrected using a cavitator not perpendicular to the trajectory.

Karimi et al [16] carried out a series of experiments on supercavitation projectile with a 7.62 mm caliber. Truncated cone was chosen as a cavitator, however, some tests failed due to lack of stability.

To the best of the author's knowledge and according to open literature, there are a few references about the accelerated bodies in cavitating regimes. The purpose of this study is to investigate unsteady supercavitating flows and evaluate the potential of available softwares and cavitation models for the prediction of such flow fields. Therefore, a series of experimental and numerical investigations are conducted that are explained in parts A and B of these papers. In the present study, i.e. part A, a setup of the experiments including prepared test tank, the characteristics of the model, some aspect of the launching system, data analysis and results are presented and compared with numerical model results.

## 2. THE EXPERIMENT SETUP

To perform the water entry and cavitation tests, a water tank is designed and installed. Canal dimensions are such that the effects of walls on the flow field would be small, i.e., 1.2 by 1.2 meters and 9 meters long. To let the model fly in two different regimes (cavitation and impact), a suitable launching system has been designed and employed. Different model velocities can be generated with variation of the gun powder of the launching system. Figure 1- depicts a typical test set-up including high speed camera (up to 36000 frame/sec), and the computer for image preserving, the test tank and the lighting system.

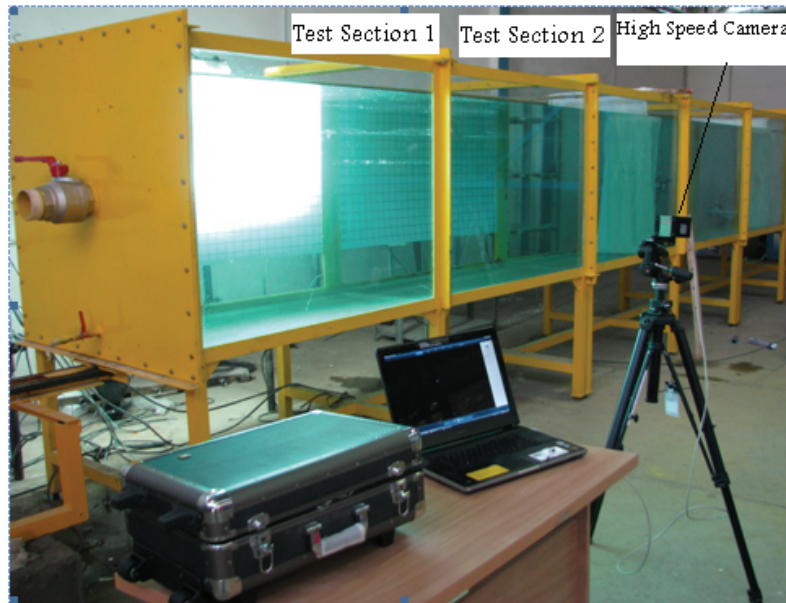


Fig. 1. A view of the experiment set up

## 3. EXPERIMENTAL INVESTIGATION OF CAVITATION AROUND A WING-BODY WITH SPHERICAL NOSE

In the first part, a model including a spherical nose and a cylindrical body is considered. Figure 2 shows the model and its cruciform fins, which are solely employed for flight stabilization.

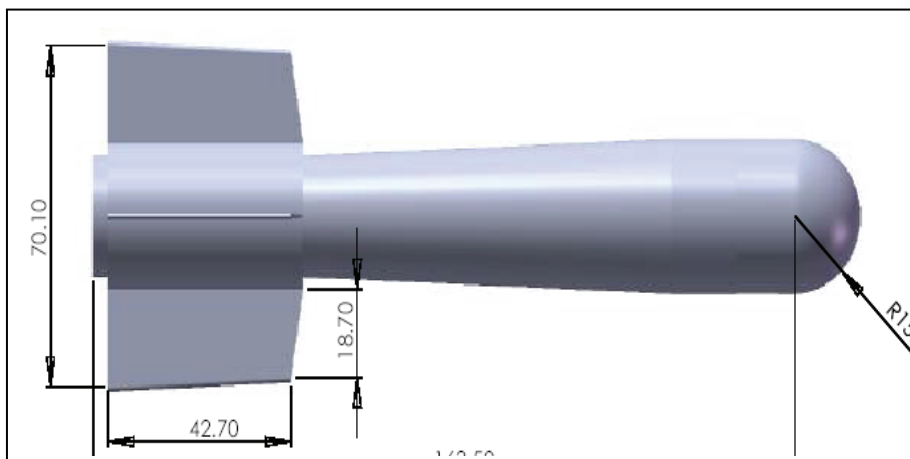


Fig. 2. Illustration of the prepared model

Stabilizers are sized to provide a calm and stable motion of the model, particularly in noncavitating regime. With careful management of the total mass and center of mass of the model ( $159.55^{\text{gr}}$  and  $6^{\text{cm}}$

from nose, respectively), the tail area is sized to provide a 2.0 caliber static margin. Some of the characteristics of the body have been summarized in Table 1.

Figures 3, 4 and 5 show a series of photographs taken by high speed camera at successive times after launch. The camera speed is set at 4000 frames per second. As can be seen, the flow about the body covers all three regimes of cavitation; inception, partial cavitation and supercavitation. Inception of cavitation and partial cavitation happens after take-off and in the accelerating stage of the flight as shown in Fig. 3. Development of supercavitation in different instants of motion are illustrated in Fig. 4. As time passes, the cavitation bubble is enhanced and the supercavitation prevails. After supercavitation regime, partial cavitation in particular, clouds cavitation owing to decreasing velocity happens again as can be seen in Fig. 5. Finally, as the deceleration goes on, all signs of cavitation disappear.

Table 1. Some of characteristics of the body

Mass	Length	Diameter	Number of Fins	Center of mass
159.55 <sup>gr</sup>	163.5 mm	15.5 mm	4	60 mm from nose

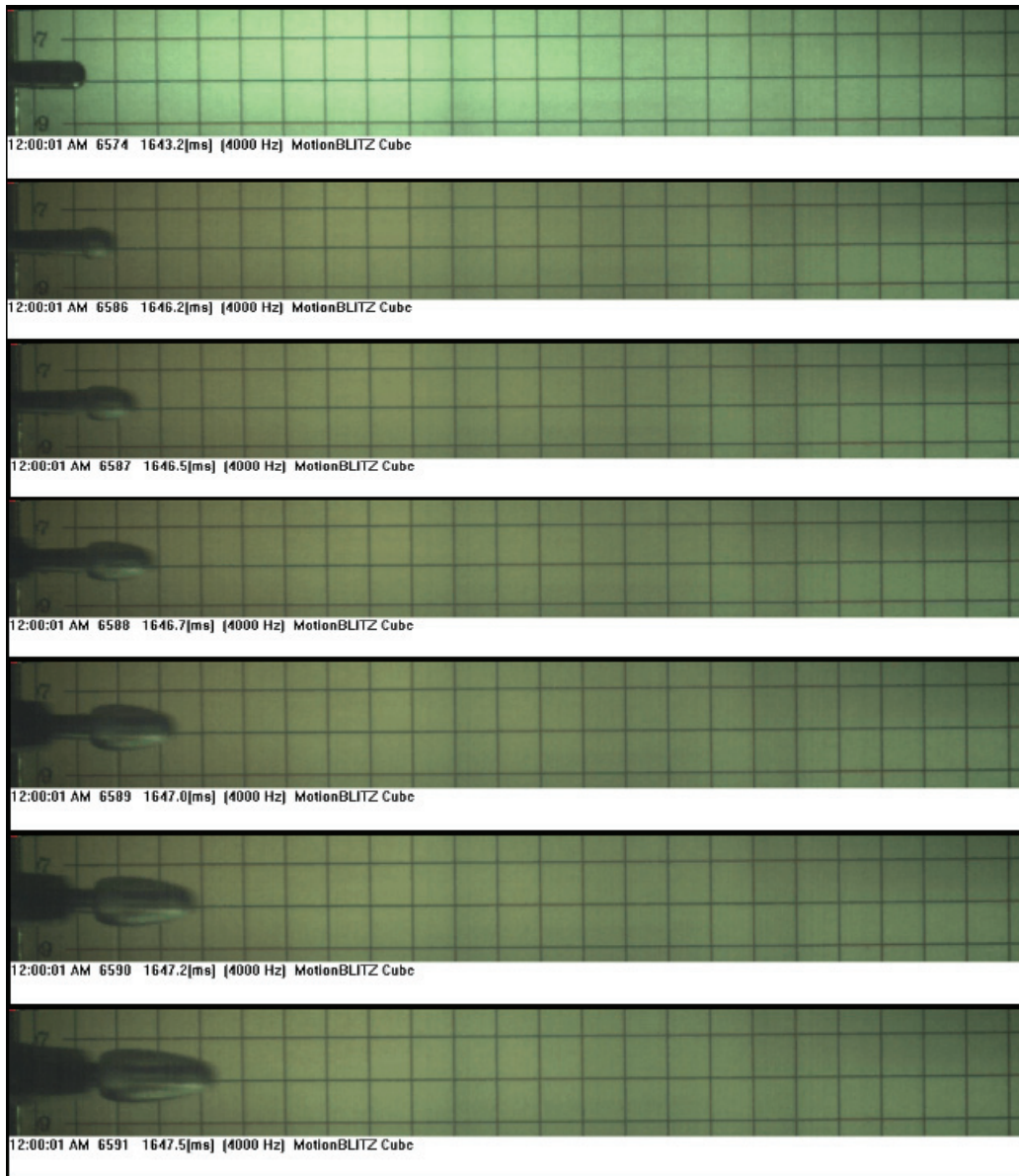


Fig. 3. Cavitation inception and partial cavitation in the accelerating phase

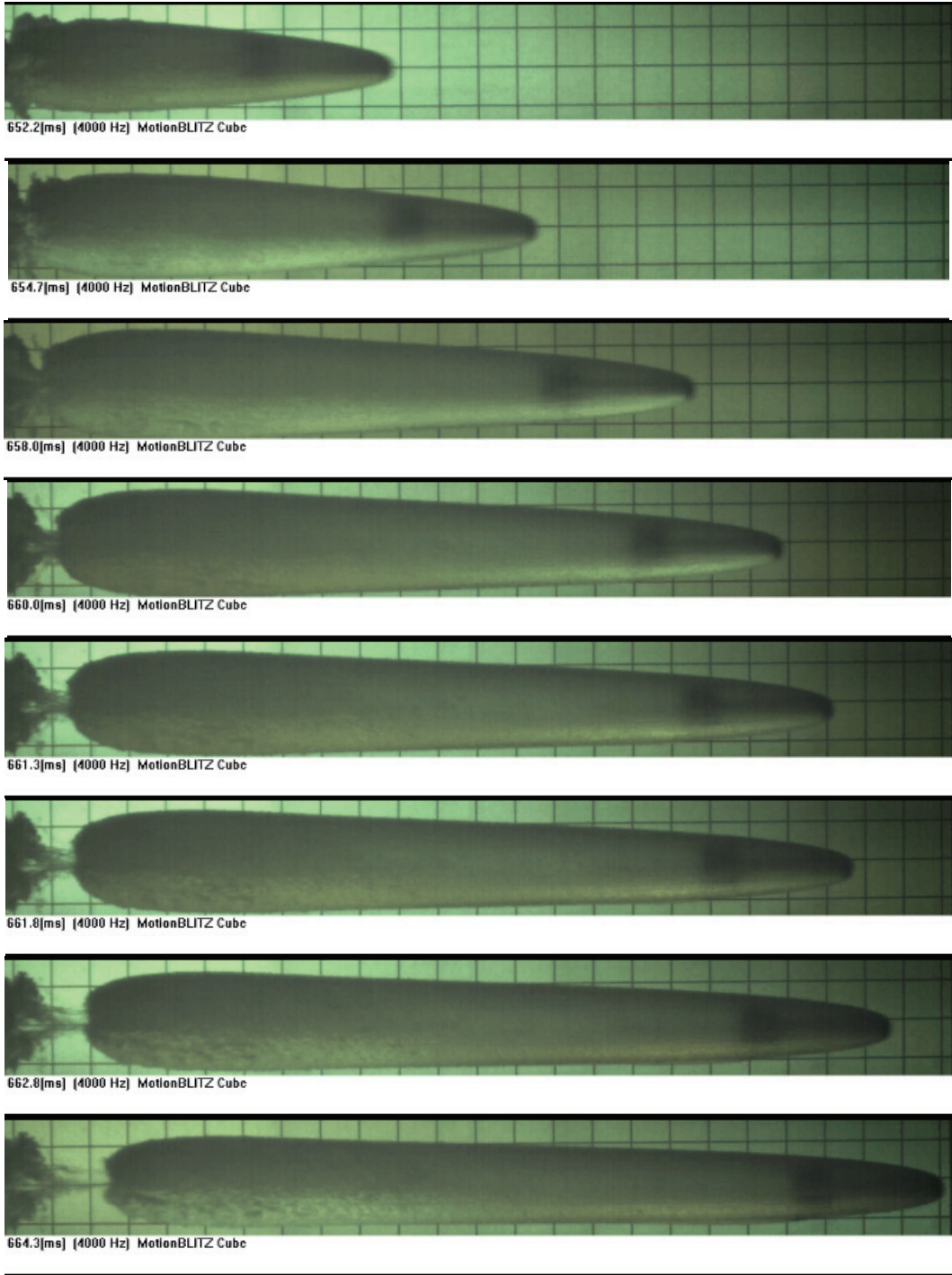


Fig. 4. Illustration of supercavitation at various times

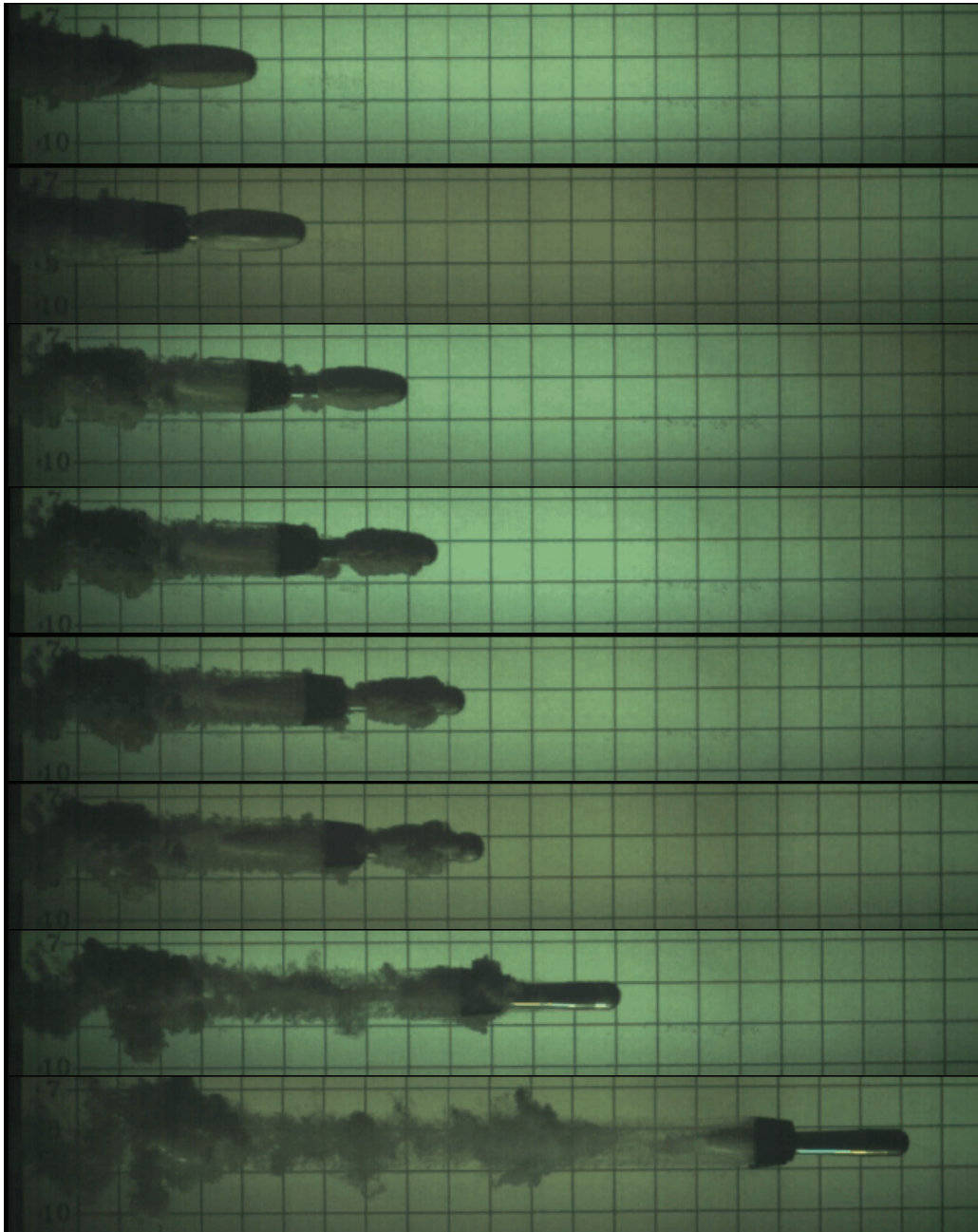


Fig. 5. Partial cavitation in the decelerating phase

#### 4. DATA PROCESSING

Different parameters are measured from the pictures taken by high speed camera. These quantities include body position, length and diameter of cavitation bubble in partial and supercavitation regimes. After processing the data, using local differences, velocity in various times and subsequently acceleration and total drag force are calculated.

Figures 6 and 7 depict position and velocity of the body versus time. As can be seen, the body gains a maximum velocity of 100(m/sec) in an approximate time of 3.0 milliseconds after movement starts. Acceleration and/or deceleration and thrust and/or total drag force are shown in Figs. 8 and 9, respectively. As can be seen, maximum order of acceleration is approximately 7000g in small time duration of the launching stage. This large amount of acceleration also indicates the importance and intricate structural design of the model.

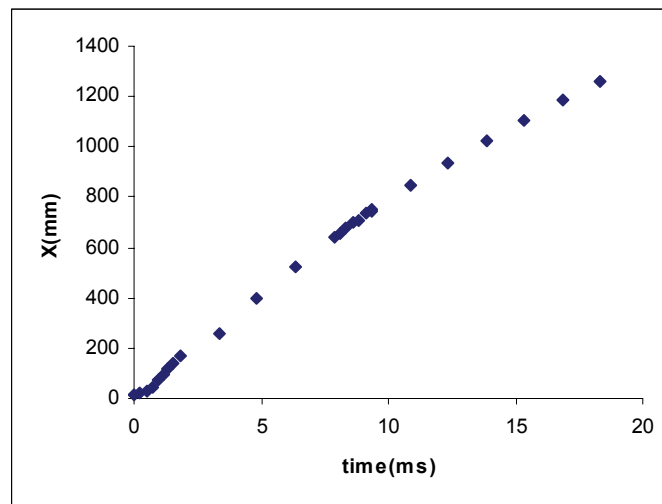


Fig. 6. Position of the body versus time

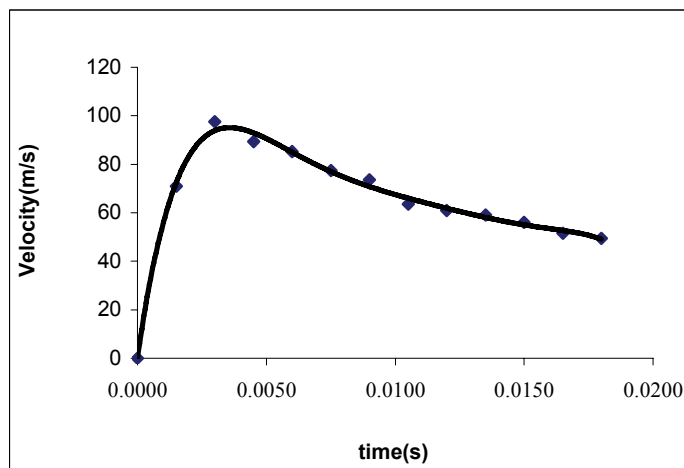


Fig. 7. Velocity of the body versus time and a curve fit for the data

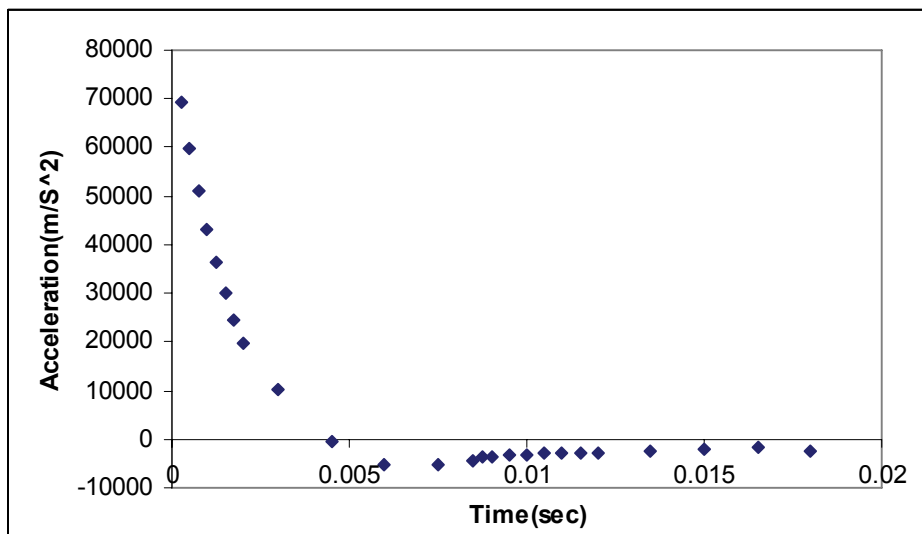


Fig. 8. Acceleration and deceleration of the body versus time

Figures 10 and 11 depict the method of measurement of length and diameter of the cavitation bubble in partial and supercavitation regimes.

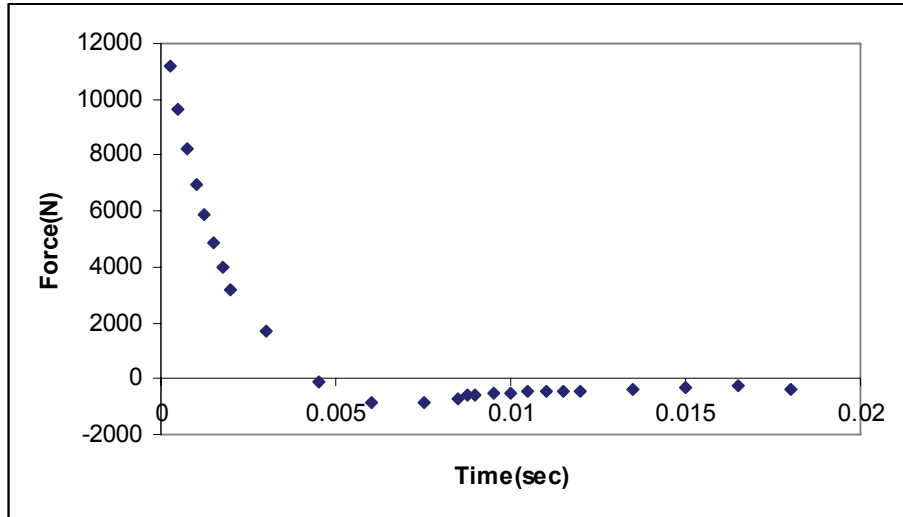


Fig. 9. Axial (positive) and total drag (negative) force versus time



Fig. 10. Measurement of bubble length in partial cavitation

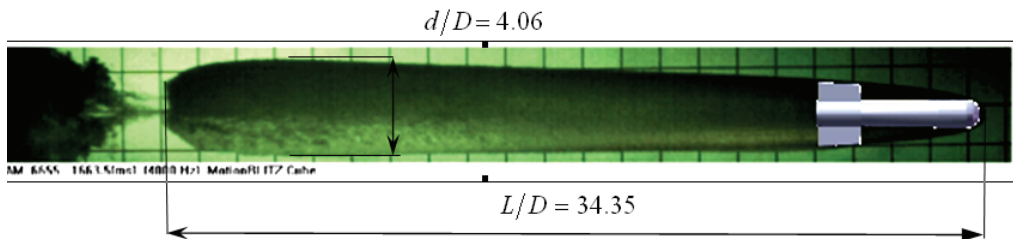


Fig. 11. Measurement of length and diameter of bubble in supercavitation

The length and diameter of the cavitation bubble in partial cavitation regime for different cavitation numbers in the accelerating phase are shown in Figs. 12 and 13, respectively. As can be seen, with increasing the velocity that is equivalent to lowering the cavitation number, the length of the cavitation bubble is increased too, which is consistent with physics. The error bounds of the experiment that are less than 1%, are also shown on these figures.

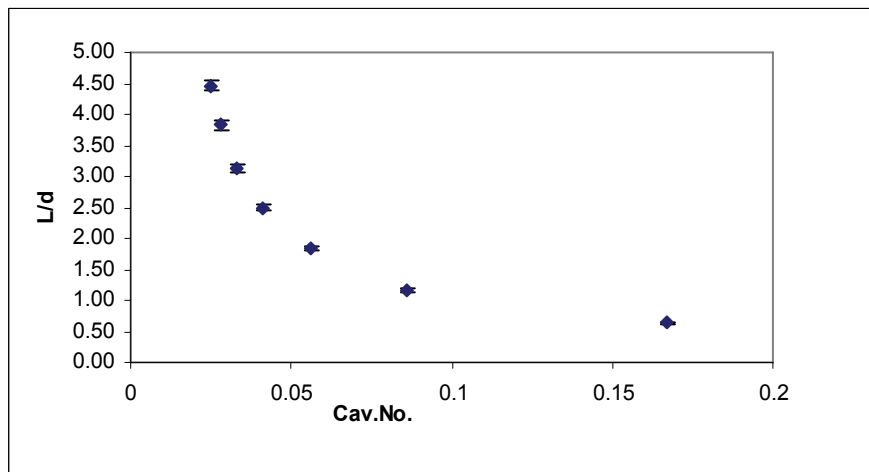


Fig. 12. Length of partial cavitation bubble versus cavitation number in accelerating phase

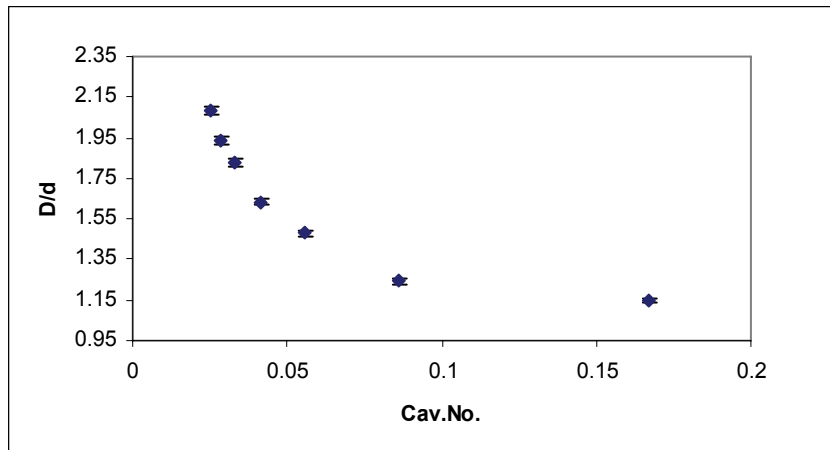


Fig. 13. Diameter of partial cavitation bubble versus cavitation number in accelerating phase

The length and diameter of the bubble in supercavitation regime for different cavitation numbers in the decelerating phase are shown in Figs. 14 and 15, respectively. As can be seen, with increasing the velocity that is equivalent to lowering the cavitation number, the length of the cavitation bubble is decreased. This matter is not consistent with the trend of cavitation bubble change in a steady state condition. In the next section this matter will be investigated more carefully, comparing the experiments with steady state numerical solution.

It should be mentioned that numerous tests with various model configurations were carried out and only the results of one test is presented here for the sake of brevity. However, one of these model modifications that has a great effect on the cavitation bubble measurement should be discussed in this section. At the end of the model a hole is provided to support the model on the launching system. The gases from the launching system that mix with the vapor in the cavitation bubble making the cavitation bubble readings erroneous are accumulated in this cavity. Therefore, it was decided to remove the end hole of the model and reduce the remained gases effect on the bubble length readings. Although no more details are presented here about this matter, the error of bubble reading would be more than 20% if this model modification was not implemented. A comparison of this modified model results with the unsteady solution is presented in part B.

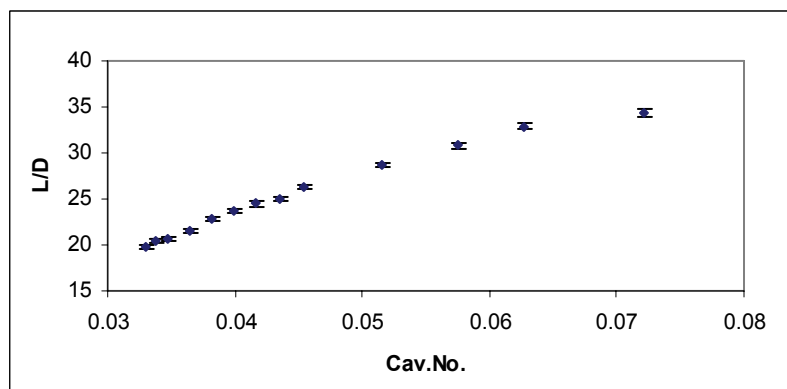


Fig. 14. The length of supercavitating bubble versus cavitation number in decelerating phase

## 5. NUMERICAL ANALYSIS

To evaluate the present experimental results, the flow field including the cavitation, is simulated numerically. As a first and ordinary model, the steady state situation is presumed. Both axisymmetric and

three-dimensional flows are considered and since the angle of attack is small in the experiments, three-dimensional effects are mainly due to stabilizers.

An available commercial CFD code, namely FLUENT, is used to compute the flow field. In the following, the numerical models of the experiments are considered. It is noteworthy that there are many references to evaluate the accuracy of the CFD code [17].

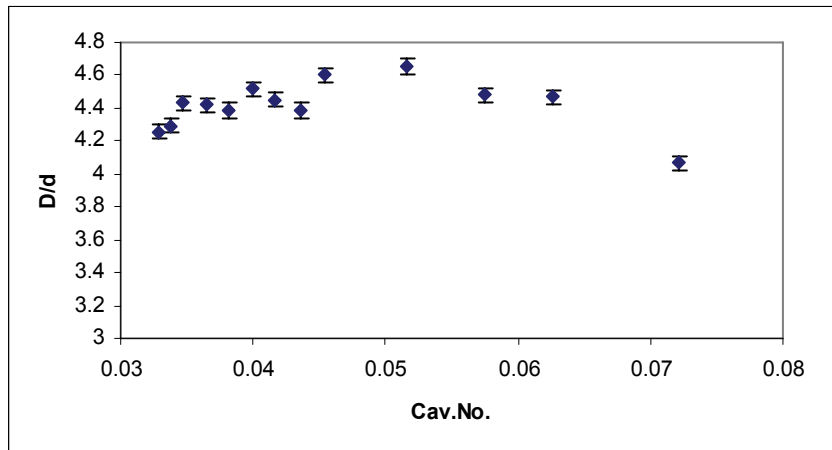


Fig. 15. Diameter of supercavitating bubble versus cavitation number in decelerating phase

## 6. THE STEADY STATE FLOW FIELD

As a simple model of the original flow field, stabilizers are removed and an axisymmetric model is considered. Notice that the stabilizers effects are restricted to the end of the model and there is no sensible influence due to the tail on the cavitation bubble unless in the supercavitation regime.

Due to flow complexities such as high density ratios of species (vapor and liquid), a tuned numerical algorithm and method should be applied. Therefore, a pressure based method together with SIMPLEC algorithm and first order upwinding is employed. Lower under-relaxation coefficients in the early stages of solution iterations provide reliable convergence.

Figures 16 and 17 illustrate the grid generated around the body and an enlargement of the grid about the nose, respectively.

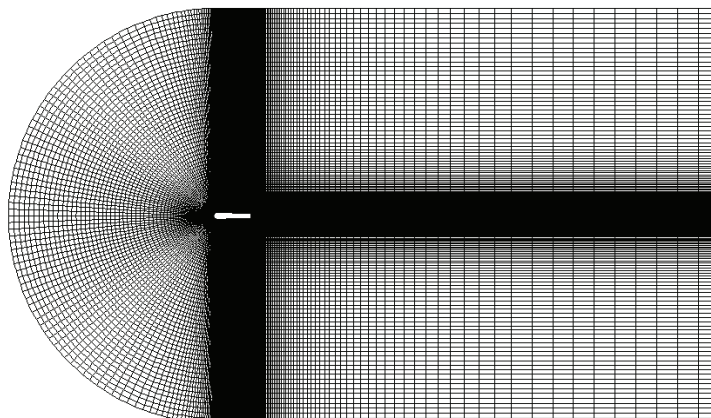


Fig. 16. An illustration of the grid

Two grid systems with 26700 and 52750 cells were used to achieve a grid independent solution. In Fig. 18, distributions of absolute pressure along the length of the body in the axial direction are shown for a cavitation number of 0.285. As can be seen, there is good agreement between the two grid system results.

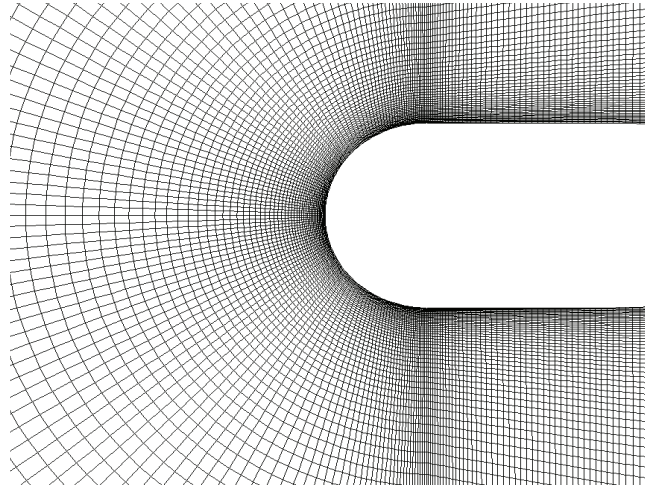


Fig. 17. An enlargement of the grid about the nose

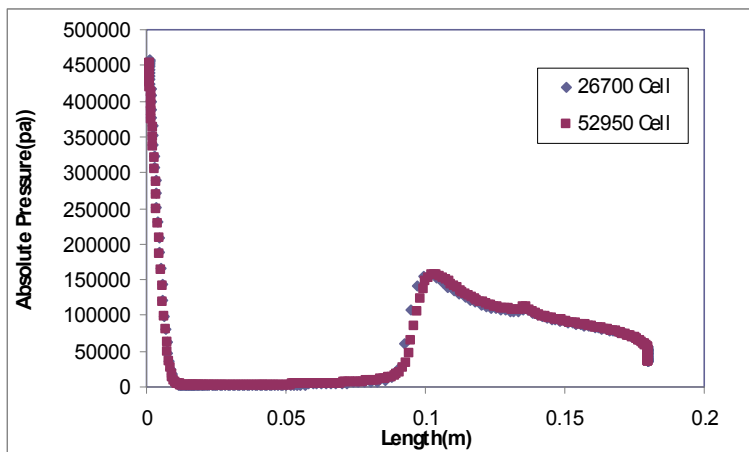


Fig. 18. Absolute pressure distribution in axial direction

Figure 19 shows volume fraction contours around the body. The length ratio of the cavitation bubble to the body diameter is 2.56.

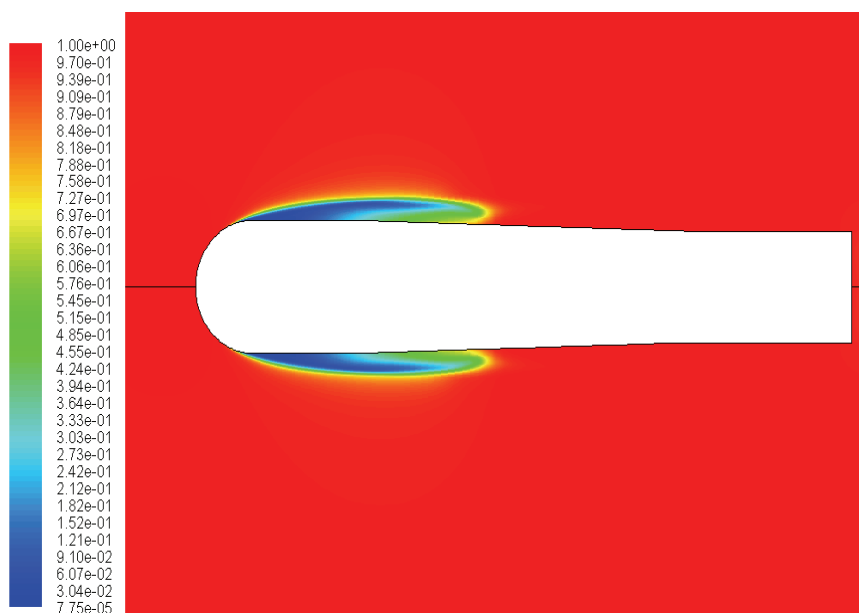


Fig. 19. Contours of volume fraction, cavitation number is 0.285

The employed turbulence model is  $k-\epsilon$  with the standard wall function. This choice requires the  $y^+$  to be in the range of  $y^+ > 11.285$ . As can be seen in Fig. 19, some part of the body is enclosed with the cavitation bubble and other parts are in contact with water that makes  $y^+$  adjustment more difficult. To satisfy this requirement the grid stretch should be fine tuned. Using the grid of Fig. 16, the final  $y^+$  range was found to be between 5 and 140 which is somewhat acceptable. In the following, the stabilizers effect on the flow field is studied in the same cavitation number of 0.285.

### 7. THREE DIMENSIONAL FLOW FIELD

Since the actual model has a tail section and these fins may affect the cavitation bubble to some extent, three-dimensional flow field including the stabilizers is studied in this section. Note that the angle of attack is small and the only effect may come from the thickness of the fins. The grid in the symmetric plane is shown in Fig. 20. Figure 21 depicts volume fraction contours at a cavitation number of 0.285. The length ratio of the cavitation bubble to the body diameter is 2.37.

Comparing the bubble length for the body alone and body plus fins, it seems that there is no essential difference in the results of the axisymmetric and the three dimension flow field at the cavitation number of 0.285. Therefore, the next flow fields are assumed as axisymmetric in the following. Note that this conclusion is limited to small angles of attack and thin fins that happen in our experiments. Also, this conclusion can be extended to lower cavitation numbers (supercavitating regime). If the fin thickness is small this is also the case.

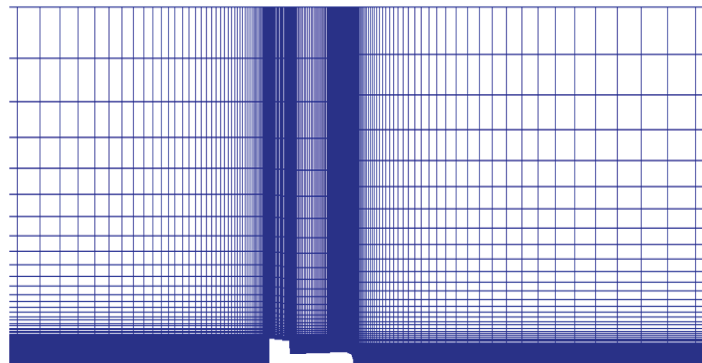


Fig. 20. An illustration of the 3-dimensional grid

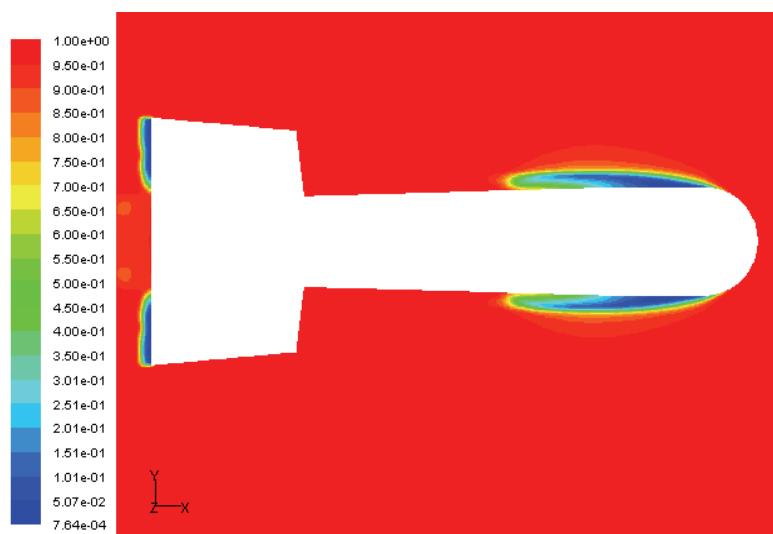


Fig. 21. Contours of volume fraction in the symmetric plane, cavitation number 0.285

## 8. COMPARISON OF RESULTS WITH THE STEADY STATE SOLUTION

In the following, the steady state flow fields at different cavitation numbers are computed and the results are compared with the obtained experimental data. The steady state model, which is usually the model of the first choice, is chosen to evaluate the importance of the unsteadiness in such flows, and is studied more carefully in part B of these papers.

Figure 22 represents the non-dimensional bubble length at different cavitation numbers at initial instants of motion (i.e., accelerating phase). As shown in this figure, there is a substantial difference between the experimental and the numerical results. Figure 23 shows contours of volume fraction in one of these cavitation numbers. Volume fraction in this cavitation number of 0.04 has enveloped the entire body, while at this cavitation number in the experimental results, the cavitation bubble covers only some part of the body as can be seen in the forth picture from the top of Fig. 5. It seems that the time history effects of the flow field, and especially acceleration, which is about 3000g on average, have an essential role on the flow field structure.

Therefore, in unsteady flows, especially those with high acceleration, the effects of the flow field history are important and must be taken into account. This subject will be investigated in length in part B.

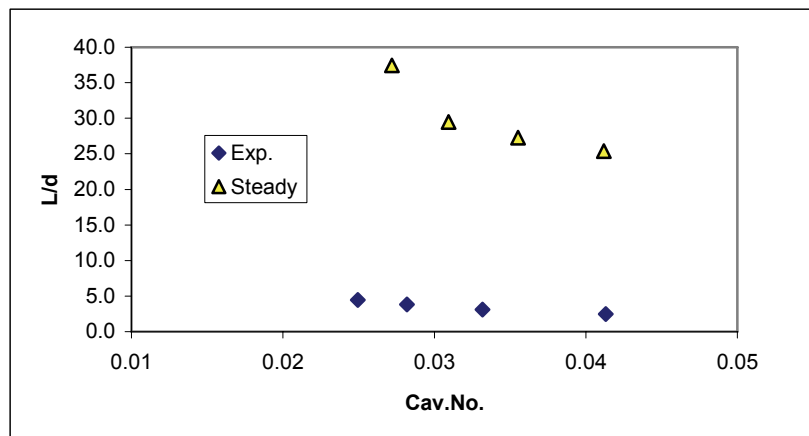


Fig. 22. Comparison of cavitation bubble length in experiment and steady state numerical solution

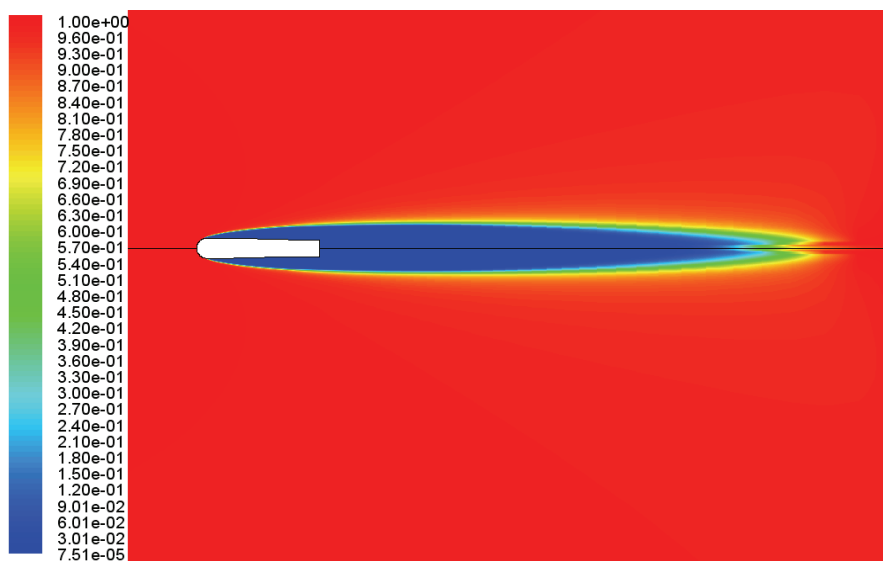


Fig. 23. Contours of volume fraction in cavitation number 0.04

## 9. CONCLUSION

In this research, multiphase fluid flows including cavitation are studied experimentally. Clear images of supercavitating bodies are collected using high speed imaging technique. At first the experimental set-up is designed and prepared to study cavitation problems. During the unsteady motion of the body and in every moment of time, the body position and development of the cavitation region are recorded.

After processing the data, the position of the body, speed, acceleration, the total drag, length, and diameter of the cavitation bubble are determined. It is shown that in the accelerating phase, with increasing the velocity that is equivalent to lowering the cavitation number, the length of the cavitation bubble that is consistent with physics is increased. Although the trend of the experiment is consistent with the numerical solution in the accelerating phase, the error magnitude is quite large (more than 600%). On the contrary, the trend of the experiment as the velocity decreases in the decelerating phase is opposite the trend of the steady solution.

It seems that in such unsteady flows, the effects of the flow field history are important and must be taken into account. However, the question remains as to what extent this flow history may affect the results. This is the subject of part B of this study.

**Acknowledgements:** The cooperation of Malek-Ashtar University of Technology in setting up the test stand and carrying out the experiments is appreciated.

## REFERENCES

1. Farzam, M. (2008). Cavitation process and the performance of some ferrous and non-ferrous alloys. *Iranian Journal of Science and Technology, Transaction B: Engineering*, Vol. 5, No. 1.
2. Knapp, R. T., Daily, J. W. & Hammitt, F. G. (1970). *Cavitation*. McGraw-Hill, New York.
3. Wang, G., Senocak, I., Shyy, W., Ikohagi, T. & Cao, S. (2001). Dynamics of attached turbulent cavitating flows. *Progress in Aerospace Sciences*, Vol. 37, pp. 551–581.
4. Nesteruk, I. (2008). Hull optimization for high-speed vehicles: supercavitating and unseparated shapes. *International Conference SuperFAST2008*. Saint-Petersburg, Russia.
5. Abelson, H. I. (1970). Pressure measurements in water-entry cavity. *J. Fluid Mech.*, Vol. 44, part 1, pp. 129-144.
6. Rouse, H. & McNown, J. S. (1948). Cavitation and pressure distribution, head forms at zero angle of yaw. *Studies in Engineering, Bulletin 32, State University of Iowa Ames, Iowa*.
7. Arakeri, V. H. & Acosta, A. J. (1973). Viscous effects in the inception of cavitation on axisymmetric bodies. *J. Fluid Eng-T. ASME*, Vol. 95, No. 4. pp. 519-527.
8. Arakeri, V. H. (1975). Viscous effects on the position of cavitation separation from smooth bodies. *J. Fluid Eng-T. ASME*, Vol. 30, No. 2, pp. 310-323.
9. Franc, J. P. & Michel, J. M. (1985). Attached cavitation and the boundary layer: Experimental investigation and numerical treatment. *J. Fluid Mech*, Vol. 154, pp. 63-90.
10. Kawanami, Y., Kato, H., Tanimura, M. & Tagaya, Y. (1997). Mechanism and control of cloud cavitation. *J. Fluid Eng-T. ASME*. Vol. 119, pp. 788-794.
11. Hrubes, J. D., Henoeh, C. W., Kirschner, I. N., Curtis, C. M. & Corriveau, P. J. (1998). NUWC Supercavitating High-Speed Bodies Test Range: Description and Test Results, *Proceedings of the 1998 ITTC Conference*.
12. Kirschner, I. N., Roth, K.W., Hrubes, J. D., Dean, L. M. & Stinebring, D. R. (1996). Progress in supercavitating high speed projectiles research. *Proceedings of the ASME & JSME Fluids Engineering Annual Conference & Exhibition, Cavitation and Multiphase Flow Forum, FED 210, San Diego, CA.9999*.
13. Li, X., Guoyu, W., Mindi, Z. & Wei, S. (2008). Structures of supercavitating multiphase flows. *International Journal of Thermal Sciences*, Vol.47, No. 10, pp. 1263-1275.

14. Hrubes, J. D. (2001). High speed imaging of supercavitating underwater projectiles. *Experiments in Fluids*, Vol. 30, pp. 57-64.
15. Schaffar, M., Rey, C. & Boeglen, G. (2005). Behavior of supercavitating projectiles fired horizontally in a water tank: Theory and experiments. *35<sup>th</sup> AIAA Fluid Dynamic Conference and Exhibit*.
16. Karimi, H., Mohammadi, J., Arabi, H., Fesanghari, R. & Farhadzadeh, F. (2008). Design, production and experiment of small caliber supercavitating projectile. *SuperFAST'2008, Saint-Petersburg, Russia*.
17. Salvador, G. & Frankel, S. (2004). Numerical modeling of cavitation using fluent: validation and parametric studies. *34th AIAA Fluid Dynamics Conference and Exhibit, Portland, USA*.